Experimental Absolute Cross-Sections for the Reaction F + D_2 at Collision Energies 90−240 meV

M. Faubel,* B. Martínez-Haya,† L. Y. Rusin,‡ U. Tappe, and J. P. Toennies

Max-Planck-Institut für Strömungsforschung, Bunsenstrasse 10, D-37073 Göttingen, Federal Republic of Germany

Received: February 4, 1997; In Final Form: March 25, 1997[⊗]

Absolute differential and integral cross-sections for the DF(v_f=0−4) vibrational products of the F + D_2(v_i=0,j_i=0−2) → DF(v_f) + F reaction have been evaluated from the time-of-flight spectra measured in high-resolution crossed molecular beam scattering experiments at five collision energies within the range 90−240 meV. The observed rise of the total reactive cross-section with increasing collision energy can be fitted with an empirical, modified line-of-centers model, yielding an activation energy of 1.8 kcal·mol^{-1}. Remarkably pronounced angular structures are observed in the vibrationally resolved differential reactive cross-sections, especially for the largest accessible vibrations, $v_f = 3$ and $v_f = 4$. The experimental absolute cross-sections are compared with the results of previously reported quantum mechanical and quasiclassical trajectory calculations on the most recent potential energy surfaces for the F + D_2 system. An overall excellent agreement is found within the experimental uncertainty. However, some significant differences are also apparent, especially at the lowest collision energies studied.

I. Introduction

The F + H_2 system has played a central role in the development of experimental and theoretical chemical dynamics and kinetics during the past 3 decades and has become a most important benchmark test for predicting interaction potential energy hypersurfaces of simple bimolecular reactions.[1]

The F + H_2 reaction and its isotopic variants have been extensively studied in a wide variety of experiments. Thermal rate constants and activation energies have been determined with different techniques.[2−6] In the late 1960s, chemiluminiscence[7,8] and laser experiments[9−11] provided the first state resolved product distributions for a chemical system. In the eighties, Lee and co-workers completed a series of pioneering experiments in which they performed the first crossed molecular beam scattering investigations,[12] determining vibrationally-resolved differential cross-sections (DCS) for the F + H_2/D_2/HD isotopic systems in the range of 29−148 meV (0.68−3.4 kcal/mol) collision energies. Similar crossed molecular beam scattering experiments have since been carried out in our laboratory in Göttingen for the F + D_2 reaction in the collision energy range 82.5−240 meV (1.9−5.5 kcal/mol). A much improved resolution yielded more accurate vibrational and rotational state resolved differential and integral reactive cross-sections.[13−24] In particular, the first absolute differential cross-sections for this reaction were determined at a 82.5 meV collision energy.[18] Furthermore, a strong dependence of the reactive differential cross-sections on the D_2 initial rotational state was experimentally observed for the first time in this system.[20] Additionally, these beam scattering experiments were extended to nonreactive elastic and inelastic collisions in order to study the long-range interaction of the F−H_2/D_2 reactants.[25,26] In another recent development, Neumark and co-workers have performed photodetachment experiments of the stable FH_2^- ion[27−29] that mainly sample the transition state region. These results complement well the crossed beam scattering experiment for the determination of the potential energy surface.

The early history of quantum chemical calculations on the F + H_2 system has been described in several reviews.[30−32] The state-of-the-art *ab initio* calculations are the 6SEC-DMBE (hereafter 6SEC)[33] potential energy surface (PES) of Truhlar and co-workers and the more recent *ab initio* SW PES calculated by Stark and Werner.[34,35] Overall, the dynamical calculations on these surfaces provide a very encouraging qualitative and quantitative agreement with the experimental results for the state resolved differential and integral cross-sections of the F + H_2 reaction and its isotopic variants.[35−44] The accuracy of the 6SEC and SW PES's has motivated a new generation of dynamical studies concerning the characterization of the collision energy dependence of the F + H_2, F + HD, and F + D_2 reaction cross-sections.[45−47]

In the present paper we report on a high-resolution crossed beam scattering study of the state resolved absolute differential and integral cross-sections of the reaction F + D_2 at five collision energies within the range 90−240 meV. After a brief description of the crossed molecular beam scattering apparatus in section II, a detailed presentation is given in section III of the analysis method used for the evaluation of the center-of-mass cross-sections from the measured time-of-flight spectra, with special emphasis on the absolute calibration of the apparatus beam intensities and detection efficiency. The reactive cross-sections are then presented and discussed in section IV, where they are also compared with the predictions of quantum mechanical and quasiclassical calculations on the 6SEC and SW potential energy surfaces. Finally, the results are summarized in section V, and general conclusions are drawn.

II. Apparatus

The crossed molecular beam scattering apparatus used in the present experiments has been described in detail in earlier publications.[18,23] Further details can be found in refs 14−16 and 19. Both the argon-seeded F-atom and the D_2 reactant beams are produced in supersonic expansions with large fluxes and high speed ratios. Each of the beams pass through three differential pumping stages before reaching the scattering region, where the background pressure is kept below 10^{-7} Torr. The DF reaction products travel over a flight path of 146 cm through four additional differential pumping stages before reaching an

† Present address: Departamento de Química Física, Universidad Complutense, E-28040 Madrid, Spain.

‡ Permanent address: Institut of Energy Problems of Chemical Physics, Leninskiĭ Prospect 38, Bldg. 2, Moscow 117829, Russia.

⊗ Abstract published in *Advance ACS Abstracts,* July 15, 1997.

S1089-5639(97)00436-2 CCC: $14.00

TABLE 1: Experimental Conditions and Characteristic Parameters of the Fluorine (10% F_2/Ar Mixture) and the Converted Deuterium (90% *ortho*-D_2, 10% para-D_2) Reactant Supersonic Beams in the Present Investigation of the F + D_2 Reaction [Source Pressure, P_0; Source Temperature, T_0; Nozzle Diameter, D_0; Gas Flux; Rotational Temperature of the D_2 Reactants, $T_{rot.}$; Degree of Dissociation of the F_2 Molecules, α; Average Beam Velocity, v_{F,D_2}; and Full-Width Spread, $\Delta v/v$]

expt.	E_{cm} (meV)	molecular beam	P_0 (bar)	T_0 (K)	D_0 (μm)	flux (Torr·L·s^{-1})	$T_{rot.}$ (D_2) (K)	α (%)	v_{F,D_2} (m/s)	$\Delta v/v$ (%)
A_1	90 ± 1.5	F	10.5	1155	65	2.0		35	1150	6
		D_2	100	295	30	29	45		2010	3
A_2	90 ± 1.5	F	2.0	1145	120	3.2		55	1145	8
		D_2	100	295	35	32	45		2010	3
B_1	111 ± 2	F	10.0	1210	75	2.4		40	1175	6
		D_2	220	380	30	60	45		2230	3
B_2	110 ± 2	F	7.0	1120	90	2.5		40	1135	6
		D_2	220	380	30	60	45		2230	3
B_3	110 ± 2	F	2.0	1145	120	3.2		55	1145	8
		D_2	100	380	35	30	65		2230	4
C_1	140 ± 3	F	5.0	1100	80	2.7		25	1130	6
		D_2	250	500	30	45	60		2620	3
C_2	140 ± 3	F	5.0	1100	90	3.4		25	1130	6
		D_2	250	500	30	45	60		2620	3
D_1	180 ± 4	F	5.0	1120	120	3.0		32	1125	6
		D_2	350	750	30	52	85		3020	3
D_2	180 ± 4	F	7.0	1200	95	2.7		41	1160	6
		D_2	350	750	30	52	85		3020	3
E_1	240 ± 5	F	8.0	1220	85	2.5		40	1165	6
		D_2	350	980	30	45	115		3530	3
E_2	239 ± 5	F	8.0	1220	85	2.5		40	1165	6
		D_2	225	980	33	35	135		3530	3
E_3	241 ± 6	F	2.5	1180	160	3.4		55	1150	8
		D_2	115	980	35	20	175		3560	4.5

electron bombardment ionizer followed by a magnetic mass spectrometer and an electron multiplier. The extensive differential pumping enables us to achieve high fluxes for the supersonic beams while keeping the background low in the scattering chamber. In addition, it prevents DF gas in the scattering chamber from reaching the detector.

The most relevant experimental parameters governing the properties of the reactant beams in the present study, such as the stagnation pressure and temperature, the gas flow, and the nozzle orifice, are listed in Table 1. Since the energy resolution of our experiment is mainly limited by the velocity spread of the fluorine atom beam, a seed gas was added to achieve a narrower velocity distribution in the supersonic expansion. A mixture of 10% F_2 in argon was used at total stagnation pressures of 2−10 bar with nozzle orifices of 65−120 μm. The typical total gas flow of 3.0 Torr·L·s^{-1} and a pressure below 1.5 mTorr was maintained in the expansion chamber by a 14 000 L/s diffusion pump. The molecular fluorine was thermally dissociated in a resistively heated magnesium fluoride oven developed in our group and described elsewhere.[48] The temperatures at the nozzle tip were in the range 1100−1220 K (see Table 1). The degree of dissociation, which was monitored by elastic scattering of F atoms and F_2 molecules from helium,[14−18,48] was found to lie between 25 and 55% in all cases (see section III.B). Fluorine beam velocities v_F = 1125−1175 m/s with full width at half-maximum (fwhm) spreads $\Delta v/v$ between 6 and 8% were measured under the present conditions.

The D_2 supersonic target beam was produced at stagnation pressures of 100−350 bar with a nozzle aperture of about 30 μm (see Table 1). A 50000 L/s diffusion pump was used to evacuate the expansion chamber so that a background pressure of somewhat less than 10^{-3} Torr could be maintained despite the large total gas flow of up to 52 Torr·L·s^{-1}. The velocity of the D_2 beam largely determines the collision energy in the center-of-mass system due to the almost five-times smaller mass compared to fluorine. By varying the D_2 beam velocity in the interval between 2010 and 3530 m/s (source temperatures T_0 = 295−980 K), collision energies in the range of E_{cm} = 90−240 meV were achieved. The half-width velocity spread of the beam was of $\Delta v_{D_2}/v_{D_2}$ = 3% in all cases. This target beam was produced in a tungsten nozzle which we assume not to catalyze *para*/*ortho* conversion at these temperatures.

As is well-known, normal deuterium is actually a mixture of two nuclear spin systems, the so-called *ortho* and *para* species. The target gas in the present experiments was a mixture of 90% *ortho* deuterium (even-*j* species) and 10% *para* deuterium (odd-*j* species) which was produced via catalyzed conversion of the normal gas at temperatures around 30 K with an efficiency of 90%.[16] Because of its high cost and the high fluxes involved in the experiments, the deuterium gas was recovered, cleaned, and recompressed in a closed cycle system. The rotational temperature of the $D_2(j_i)$ reagent molecules in the beam was estimated by means of the expression

$$\log(T_{rot.}/T_0) = -0.44 \log\left(\frac{P_0 D_0}{T_0^{1/2}}\right) - 0.32 \qquad (1)$$

which provides a best linear fit to the experimental data of Pollard and co-workers.[23,49] This expression is consistent within 5% with the similar type of fit introduced in ref 50 for T_0 = 293 K, but it differs by roughly 25% from the expression employed for T_0 = 500−980 K in previous publications,[20,22] where $\log(P_0D_0/T_0)$ was used in the right hand side of eq 1, as suggested in ref 50. According to eq 1, the rotational temperature of the D_2 beam lies in the range $T_{rot.}$ = 45−175 K for the different experiments of the present study (see Table 1). The corresponding relative rotational populations are listed in Table 2, where it can be seen that j_i = 0 is the most populated rotational state in all experiments but one. Only at the highest collision energy, at 240 meV (experiment E3), the j = 2 state shows the highest population.

The deuterium beam was modulated during the scattering experiments using a pseudorandom 255-slit sequence with an overall time-of-flight (TOF) window of 1.79 ms. Depending on the scattered intensity, the total measuring time for each time-of-flight spectrum of the DF products varied between 6 and 16 h. The investigation of a given collision energy was completed

TABLE 2: Relative Rotational Populations, $\rho(j_i)$, of the D_2 Reagents at the Estimated Rotational Temperatures, $T_{rot.}$, of the Present Experiments Listed in Table 1[a]

expt	E_{cm} (meV)	$T_{rot.}$ (K)	$\rho(j_i=0)$	$\rho(j_i=1)$	$\rho(j_i=2)$	$\rho(j_i\geq 3)$
A_1, A_2	90	45	0.90	0.10	0.00	0.00
B_1, B_2	110	45	0.90	0.10	0.00	0.00
B_3	110	65	0.84	0.10	0.06	0.00
C_1, C_2	140	60	0.85	0.10	0.05	0.00
D_1, D_2	180	85	0.74	0.10	0.16	0.00
E_1	240	115	0.59	0.09	0.31	0.01
E_2	240	135	0.52	0.09	0.37	0.02
E_3	240	175	0.41	0.08	0.47	0.04

[a] A converted mixture with 90%/10% *ortho*-D_2/*para*-D_2 was used in all cases.

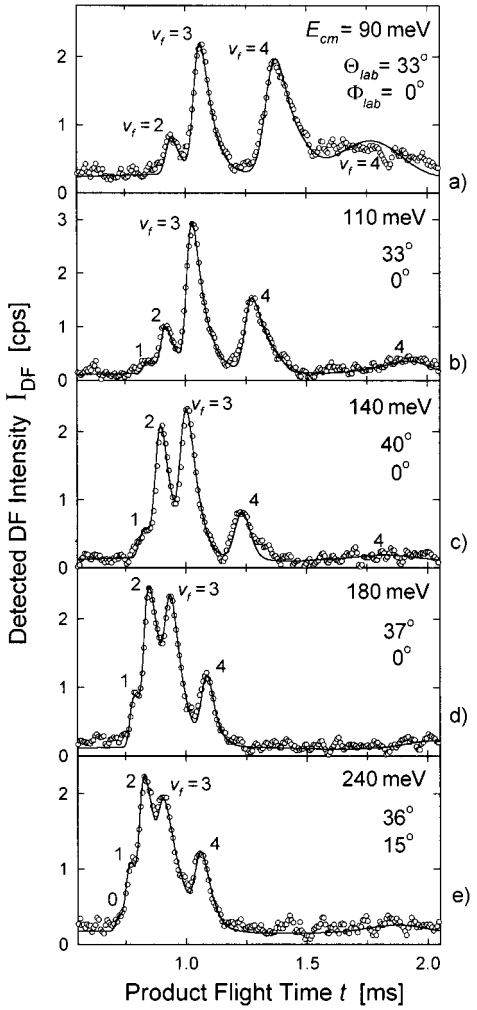

Figure 1. Five typical time-of-flight spectra of the DF products of the F + D_2 reaction measured at collision energies, E_{cm}, and laboratory scattering angles, Θ_{lab} (in-plane angle) and Φ_{lab} (out-of-plane): (a) E_{cm} = 90 meV, Θ_{lab} = 33°, Φ_{lab} = 0°; (b) 110 meV, 33°, 0°; (c) 140 meV, 40°, 0°; (d) 180 meV, 37°, 0°; (e) 240 meV, 36°, 15°. The vibrational state of the DF molecule, v_f = 0−4, associated with each peak in the spectra is indicated. The circles (○) denote the measurements, and the solid curves represent the best-fit simulation of each spectrum.

in a series of 2−3 experimental runs, each of them involving the measurement of typically about 10 TOF spectra. The TOF spectra of Figure 1 were repeated in regular intervals together with measurements of the F and D_2 beam velocities and of the degree of dissociation of the F beam in order to account for the different experimental conditions at the respective collision energy and to control possible deterioration of the scattering conditions during the course of each experiment. Additionally, Ar−D_2 elastic scattering intensities were measured at several angles with the same Ar/F_2 mixture to monitor the intensity and stability of both beams and of the scattering and detecting conditions. The Ar−D_2 scattering system was also used for the absolute calibration of the reactant beam intensities and for the determination of the absolute sensitivity of the detector, as described in section III.B.

III. Analysis

III.A. Time-of-Flight Spectra. Typical time-of-flight spectra of the DF products are shown in Figure 1 for each of the collision energies studied in the present work. Typically, 25−30 spectra were measured at each collision energy covering the relevant range of scattering angles. The laboratory (LAB) scattering angles Θ_{lab} (angle in the reactant plane) and Φ_{lab} (out-of-plane angle) are defined in ref 18. Even though all center-of-mass (CM) scattering angles of any two-body collision process can be studied in the plane of the two incident beams, the energy resolution can be significantly improved by taking advantage of the out-of-plane geometries.[18] The optimum product energy resolution (fwhm) in the TOF spectra ranges between 20 (E_{cm} = 90 meV) and 40 meV (E_{cm} = 240 meV), which allows one to clearly resolve all five accessible DF vibrational states from $v_f = 0$ to $v_f = 4$. The product vibrational states associated with the respective time-of-flight peaks in the spectra are indicated in Figure 1.

The measured time-of-flight spectra were analyzed by means of a three-dimensional forward convolution for the time-dependent intensity at a given laboratory scattering direction, $I(\Theta_{lab},\Phi_{lab},t_n)$:[22,23,42]

$$I(\Theta_{lab},\Phi_{lab},t_n) = n_F^{\circ} n_{D_2}^{\circ} \epsilon(DF)\, \hat{I}(\Theta_{lab},\Phi_{lab},t_n) \qquad (2)$$

where n_F° and $n_{D_2}^{\circ}$ are the absolute average number densities of the reagent beams in the scattering center and $\epsilon(DF)$ is the efficiency for DF detection. The product $n_F^{\circ} n_{D_2}^{\circ} \epsilon(DF)$ was determined by a calibration procedure described below. Finally, $\hat{I}(\Theta_{lab},\Phi_{lab},t_n)$ is given by

$$\hat{I}(\Theta_{lab},\Phi_{lab},t_n) = \int d^3\mathbf{r}\, \hat{n}_F(\mathbf{r})\, \hat{n}_{D_2}(\mathbf{r}) \int d\Omega\, D(\Omega;\Theta_{lab},\Phi_{lab}) \int\int dv_F\, dv_{D_2} \times f(v_F)\, f(v_{D_2}) g \sum_{j_i} \rho(j_i) \sum_{q=1,2} \sum_{p} \left(\frac{d\sigma}{d\omega}\right)_{pq} \left|\frac{d\omega}{d\Omega}\right|_{pq} \frac{1}{v_{pq}} F(t_n)$$

$$\left|\frac{d\omega}{d\Omega}\right|_{pq} = \frac{v_{pq}^2}{u_p^2 |\cos\xi_{pq}|}$$

$$F(t_n) = H[\tau_{pq} - t_n]\, H[(t_n+\delta) - \tau_{pq}] \qquad (3)$$

The multiple integrals were calculated by a Monte Carlo sampling of the velocities and the spatial densities of the F and D_2 reagents, determined by the experimental beam velocity profiles and angular divergences:

$$f(v_\lambda) = N_v v_\lambda^2 \exp\left\{-\left(\frac{v_\lambda - v_\lambda^{\circ}}{\delta v_\lambda}\right)^2\right\}$$

$$\hat{n}_\lambda(\mathbf{r}) = N_\gamma \exp\left\{-\left(\frac{\gamma(\mathbf{r})}{\delta\gamma_\lambda}\right)^2\right\}$$

λ denotes the F or the D_2 beam, respectively. The normalized velocity distribution of the reactant beams, $f(v_\lambda)$, is characterized by the most probable velocities, v_λ°, and full widths at half-maximum, $\Delta v_\lambda = 2(\ln 2)^{1/2} \delta v_\lambda$. The position vector $\mathbf{r}$ refers to

a point of the beam intersection volume in which the density distribution of each reactant, $\hat{n}_\lambda(\mathbf{r})$, is represented by a normalized Gaussian distribution of full width $\Delta_\gamma = 2(\ln 2)^{1/2}\delta_\gamma$, which is determined by the angular divergence of the reactant beams. (Actual values are $\Delta_\gamma = 1.6°$ for the F atoms and $\Delta_\gamma = 2.0°$ for the D_2 beam, respectively.) N_v and N_γ are normalization factors, respectively.

The remaining notation in eq 3 is as follows: $\rho(j_i)$ is the initial relative population of the j_i rotational states of D_2 (Table 2), g is the relative velocity of the reactants, $(d\sigma/d\omega)_{pq}$ is the center-of-mass differential cross-section for a product molecule in the $p(=v_f,j_f)$ rovibrational state, and v_{pq} is its final velocity in the laboratory frame. The additional subindex $q = (+ \text{ or } -)$ denotes product center-of-mass velocities u_p which are directed either to the right or to the left of the relative velocity, g, leading to "fast" and "slow" products in the laboratory frame, respectively;[51] ξ_{pq} is the angle between v_{pq} and u_p. The integral over the solid angle, Ω, accounts for the cone of acceptance of the detector, represented by the function $D(\Omega;\Theta_{lab},\Phi_{lab})$. The factor $1/v_{pq}$ in eq 3 accounts for the number-density sensitivity of the electron-bombardment ionization detector. Finally, the measured total flight time, $\tau_{pq} = t_{DF} + t_{D_2} + t_{ion}$, is the sum of the flight time of the DF product molecule in the corresponding internal state from the scattering center to the ionization region, t_{DF}, plus the flight times of the D_2 reagent from the chopper to the scattering center, t_{D_2}, and of the molecular ion DF+ inside the mass spectrometer toward the electron multiplier, t_{ion}. A time window $[t_n, t_n + \delta]$ is associated with each time-of-flight channel in the experiment, where t_n and $\delta = 7$ μs are, respectively, the time and full width of the nth channel ($n = 1-255$, $t_1 = 0.532$ μs, $t_{255} = 2.310$ μs). The product $F(t_n)$ of Heaviside step functions $H(x)$ (equal to 1 for positive x and equal to zero for negative x) assures that only products within the corresponding time windows contribute to a given channel.

The initial relative rotational populations corresponding to each experiment, as listed in Table 2, were taken for the $\rho(j_i)$ weights. The internal energy of each initial rotational state was simply added to the reaction exothermicity (1.382 eV = 31.86 kcal/mol). Thus, the measured v_f, j_f state resolved differential cross-sections can be interpreted as averages over the particular initial rotational state distribution of each experiment.

In the present analysis, and as in our previous work,[18,20,22,23] only fluorine atoms in their $P_{3/2}$ ground state were assumed to take part in the reaction. At a typical fluorine-source operating temperature of 1150 K, around 23% of the atoms produced are estimated to be in the $^2P_{1/2}$ excited fine-structure state, which lies about 50 meV above the ground state. Although evidence for the reactivity of $^2P_{1/2}$ fluorine has been reported at a collision energy slightly below the range here studied (83.5 meV),[18,19,23] the reactive cross-section for this excited state was measured to be at least 1 order of magnitude smaller than for the reaction from $^2P_{3/2}$ ground state atoms. In view of this small cross-section and since all the measured TOF spectra could be correctly fitted without any reactive contribution from the $^2P_{1/2}$ state, this channel was neglected altogether.

The differential cross-section for each product vibrational and rotational state, $(d\sigma/d\omega)_{v_f,j_f}$, was constructed using the following scheme:

$$(d\sigma/d\omega)_{v_f,j_f}(\theta_{cm}) = \sum_k A_k(v_f)\, P_k(j_f;v_f)\, G_k(\theta_{cm}) \qquad (4)$$

with

$$\sum_{j_f} P_k(j_f;v_f) = 1$$

$$G_k(\theta_{cm}) = H[(\theta_{cm} - (\theta_{cm}{}^k - \Delta)]\, H[(\theta_{cm}{}^k + \Delta) - \theta_{cm}]$$

Here $\theta_{cm} = 0°$ corresponds to a DF product center-of-mass velocity in the direction of the initial velocity of the F atom (forward scattering), whereas $\theta_{cm} = 180°$ is directed opposite to the incident F atom (backward scattering). The trial $(d\sigma/d\omega)_{v_f,j_f}$ functions were structured in discrete boxes corresponding to the intervals of center-of-mass scattering angles $[\theta_{cm}{}^k - \Delta, \theta_{cm}{}^k + \Delta]$ of half-width $\Delta = 1.5°$ and average scattering angle $\theta_{cm}{}^k = (2k - 1)\Delta$, where the index k ($k = 1-60$) denotes the kth box. The function $G_k(\theta_{cm})$ in eq 4, which is a product of two Heaviside step functions similar to $F(t)$ in eq 3, projects out a uniform cross-section, given by the product $A_k(v_f)\, P_k(j_f;v_f)$, for each of the discrete angular intervals. Three adjustable parameters, different for each product vibrational state, are associated with each interval: $A_k(v_f)$, the total differential cross-section at the corresponding scattering angle, and two additional parameters that determine the maximum and the width of the product rotational probability distribution $P_k(j_f;v_f)$, as described in refs 22−24. For backward scattered DF products in the vibrational states $v_f = 2$ and $v_f = 3$ at low collision energy, $E_{cm} = 90$ and 110 meV, bimodal rotational distributions were required which were constructed with the expression $(d\sigma/d\omega)_{v_f,j_f} = A^{(1)}(v_f;\theta_{cm})\, P^{(1)}(j_f;v_f\theta_{cm}) + A^{(2)}(v_f;\theta_{cm})\, P^{(2)}(j_f;v_f\theta_{cm})$, involving two independent two-parameter j_f distributions, $P^{(1)}$ and $P^{(2)}$.[23,24]

The best-fit parameters of the center-of-mass differential cross-sections $d\sigma/d\omega$ were determined by trial and error calculations via eq 2 of the measured TOF spectra of the DF products. In Figure 1 the corresponding best-fit simulations, shown as solid lines, are compared with representative TOF measurements for the five collision energies investigated. The agreement between the simulated and the measured spectra is very good, the location and shape of the observed vibrational time-of-flight peaks being well-reproduced in all cases, as shown in greater detail previously.[20,22−24]

III.B. Absolute Calibration. The determination of *absolute* differential cross-sections from the time-of-flight measurements by means of eq 2 in principle requires the knowledge of the absolute values of the density of the F and D_2 reactants in the scattering center and of the efficiency of detection of the DF products. In the present work an alternative method has been followed which is based on an additional nonreactive Ar−D_2 scattering experiment calibration. The Ar−D_2 interaction is well-characterized, and absolute differential cross-sections for elastic scattering and for rotational excitation of the D_2 molecules are well-known.[52] The Ar−D_2 system also has the advantage that it can be investigated simultaneously and under the same conditions as those for the F−D_2 reactive experiment, since Ar constitutes about 90% of the seeded F beam.

With the same notation as that in eq 2, the time-of-flight spectra measured in the Ar−D_2 scattering experiments are analyzed with the following expression:

$$I_{Ar}(\Theta_{lab},\Phi_{lab},t_n) = n_{Ar}{}^\circ n_{D_2}{}^\circ \epsilon(Ar)\, \hat{I}_{Ar}(\Theta_{lab},\Phi_{lab},t_n) \qquad (5)$$

By comparing the detected signal, I_{Ar}, with the Monte Carlo evaluation of $\hat{I}_{Ar}$, for the calculated Ar−D_2 absolute differential cross-sections the absolute value of the product $n_{Ar}{}^\circ n_{D_2}{}^\circ \epsilon(Ar)$ was first determined. Then, the product $n_F{}^\circ n_{D_2}{}^\circ \epsilon(DF)$ for the reactive scattering experiment in the *same* conditions for beam production and product detection was calculated by rewriting $n_{D_2}{}^\circ$, using eq 5:

$$n_F{}^\circ n_{D_2}{}^\circ \epsilon(DF) = \frac{n_F{}^\circ}{n_{Ar}{}^\circ} \frac{\epsilon(DF)}{\epsilon(Ar)} \frac{I_{Ar}}{\hat{I}_{Ar}} \qquad (6)$$

Thus, the F−D_2 absolute differential reactive cross-sections are determined from the analysis of the TOF measurements, $I_{DF}(\Theta_{lab},\Phi_{lab},t_n)$ with the following expression, formally equivalent to eq 2:

$$I_{DF}(\Theta_{lab},\Phi_{lab},t_n) = n_F^\circ n_{D_2}^\circ \epsilon(DF)\,\hat{I}_{DF} = \frac{n_F^\circ}{n_{Ar}^\circ}\frac{\epsilon(DF)}{\epsilon(Ar)} C_{Ar}\hat{I}_{DF} \tag{7}$$

where the dependence of $C_{Ar} \equiv I_{Ar}/\hat{I}_{Ar}$ and of $\hat{I}_{DF}$ on $(\Theta_{lab},\Phi_{lab},t_n)$ has been omitted to simplify the notation. The determination of the *relative* density, n_F°/n_{Ar}°, and the *relative* detection efficiency, $\epsilon(DF)/\epsilon(Ar)$, are described below in this section. The former ratio is measured *in situ*, whereas the latter one has to be estimated from previously published experimental and theoretical data.

The density of reactants in the scattering volume is determined by the respective D_2, F_2, and Ar beam source conditions and by the F-atom source dissociation and survival probability in the molecular beam formation process.

The thermal dissociation of the F_2 molecules at *constant pressure* in the beam source changes slightly the composition of the gas mixture. For our present mixture, of 10% F_2 in Ar, for a given degree of dissociation, α, the F/Ar density ratio in the source is given by the following expression:

$$\frac{n_F^{(s)}}{n_{Ar}^{(s)}} = \frac{0.22\alpha}{1 - 0.11\alpha} \tag{8}$$

For an effusive molecular beam, the density of fluorine atoms relative to that of argon atoms would be the same in the scattering center as in the source. In a nonideal real free jet expansion, however, several factors can induce variations in the final composition of the beam with respect to the source conditions:

(i) The interaction of the species of the mixture with the background gas in the expansion chamber can induce a significant intensity attenuation, prior to the extraction of the beam. This process should, in principle, be more effective for Ar because of its larger cross-section compared to the F atoms. According to *Beer's law* the intensity at a distance l from the nozzle source is $I(l) = I_0 \exp(-nl\sigma)$, where $I_0 \equiv I(l = 0)$, n is the density of the background gas, and $\sigma_{Ar(F)}$ are the total cross-sections for scattering of the Ar and F atoms from the background gas. With the typical values $\sigma_{Ar} \approx 0.36 \times 10^{-18}$ m^2, $\sigma_F \approx 0.24 \times 10^{-18}$ m^2,[53] and $n \sim 3.2 \times 10^{19}$ m^{-3} (background pressure of 1 mTorr), $l \approx 2$ cm (flight path from the nozzle to the first collimator), we estimate: $(I/I_0)_{Ar} \approx 0.93(I/I_0)_F$.

(ii) Another important aspect is the possible interference of the expanding gas with the conical skimmer used to extract the beam.[54] It is difficult to quantify the magnitude of this effect, which, in general, tends to affect largely the lighter species, in this case the F atoms. In the present experiments, a new commercially available skimmer[55] with better transmission properties was used for both beams. The factor of 2 increase in beam flux with respect to our previous experiments[23] suggests a significant reduction in beam interference. Thus, it is reasonable to assume a similar intensity attenuation for both F and Ar atoms (within 10% in the worst case) due to skimmer interference.

(iii) The asymptotic velocity of the F atoms in the beam under the present conditions, due to the lower mass, is about 2% larger than for the Ar atoms.[66] This reduces the relative density of F in the beam by about 2% with respect to the Ar density.

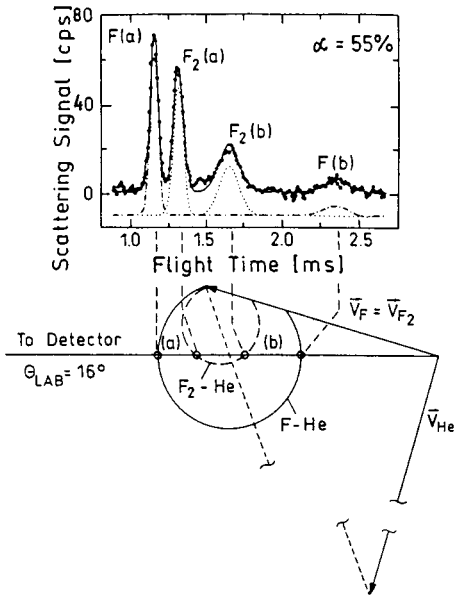

Figure 2. Typical time-of-flight spectrum of the elastic scattering of F atoms and F_2 molecules from helium used to determine the degree of dissociation of the fluorine beam, α (55% in this example). A reversed Newton diagram is also shown in the lower part of the figure for direct comparison with the time-of-flight axis and identification of the experimental peaks.

(iv) Finally, in a nonideal supersonic expansion of a binary gas mixture the velocity distribution in the direction perpendicular to the beam axis tends to be broader for the lighter species. The asymptotic perpendicular speed ratio follows approximately the relation $S_\perp \propto (m/T_\perp)^{1/2}$,[67] where m is the corresponding molecular (or atomic) mass and $T_\perp$ is the effective perpendicular temperature, which is the same for both species. Consequently, in the F/Ar beam of the present experiments, a slightly larger angular divergence is to be expected for the F than for the Ar atoms. The angular divergence (fwhm) of the Ar and D_2 beams in the present experiments is typically $\Delta\gamma = 1.5°$. From Ar−He and F−He scattering experiments we found that the angular divergence of the F beam in the same conditions is at most $\Delta\gamma_F \leq 1.8°$. In any case, the variation of $\Delta\gamma_F$ between 1.5 and 2.0° induces changes of less than 10% in the absolute calibration.

Summarizing, the effects mentioned in i−iv above partially cancel each other and account, altogether, for a possible change of the Ar/F density ratio of less than 10%. In view of this, it has been assumed throughout the present analysis that the relative density maintains approximately the same value in the scattering volume as in the thermal source, $n_{Ar}^\circ/n_F^\circ \approx n_{Ar}^{(s)}/n_F^{(s)}$.

A measurement of the fractional dissociation $\beta \equiv n_F/n_{F_2}$ allows one to determine the degree of dissociation of the beam, $\alpha \equiv \beta/(2 + \beta)$. α cannot be determined from its equilibrium value in the source since it very likely changes during the Ar-seeded supersonic expansion of the fluorine.[48] β was therefore measured by kinematical separation of the atomic and the molecular fluorine species in elastic scattering from helium.[18,23,48] Figure 2 shows typical F−/F_2−He elastic scattering time-of-flight spectra, showing a clear separation of elastically scattered F and F_2.

A Newton diagram representing the experimental kinematical conditions is shown in Figure 2 and helps to identify the time-of-flight peaks. The density ratio of both species is determined from the following expression:

$$\frac{n_F}{n_{F_2}} = \frac{\epsilon^{19}_{F_2}}{\epsilon_F} \cdot \frac{(d\sigma/d\omega)_{F_2}}{(d\sigma/d\omega)_F} \frac{|d\omega/d\Omega|_{F_2}}{|d\omega/d\Omega|_F} \frac{v_F}{v_{F_2}} \frac{I_F}{I_{F_2}} \qquad (9)$$

Equation 9 involves the ratio of the ionization cross-sections for dissociative ionization of F_2 to F^+ and of direct ionization of F to F^+, $\epsilon^{19}_{F_2}/\epsilon_F \approx 0.51$;[18,70,71] the cross-sections of the F_2-He and F−He elastic scattering processes in the center-of-mass system, $(d\sigma/d\omega)_{F_2,F}$; and the ratio of the Jacobi factors of the transformation from the laboratory to the center-of-mass coordinate system, $|d\omega/d\Omega|_{F_2(F)}$. The ratio I_F/I_{F_2} represents the measured scattering intensities, i.e., the areas under the detected scattered time-of-flight peaks measured with the mass spectrometer detector at mass 19. The ratio v_F/v_{F_2} of the final laboratory velocities corrects for the density-proportional efficiency for electron impact ionization.

The largest uncertainty in the determination of the degree of dissociation by eq 9 arises from the estimation of the ratio of the center-of-mass differential cross-sections, $(d\sigma/d\omega)_{F_2}/(d\sigma/d\omega)_F$. Aquilanti and co-workers have determined empirically a potential energy surface for the F + He system.[69] However, to date, the F_2-He interaction has not been characterized with enough accuracy for the direct determination of the differential cross-sections for elastic scattering. According to a simple spherical hard shell model, for a given center-of-mass angle, the cross-section for F_2 scattering should be a factor of $2^{2/3}$ larger than for scattering of F atoms because of the difference in sizes. We must also account for the fact that in the time-of-flight spectrum of Figure 2 at $\Theta_{lab} = 16°$, the peak for F atoms belongs to a smaller center-of-mass scattering angle ($\theta_{cm} \approx 75°$) than the peak for F_2 ($\theta_{cm} \approx 125°$), as can be seen in the Newton diagram included in the lower panel of the figure. For realistic potentials, we thus expect the F-atom cross-section to be larger. Simple model estimates suggest that these effects should roughly cancel, so that $(d\sigma/d\omega)_{F_2-He}(125°) \approx (d\sigma/d\omega)_{F-He}(75°)$. This is, indeed, found to be the case for the elastic scattering of systems with masses and sizes similar to F_2-He/F−He, such as Ar−He/Ne−He,[16] Ar−D_2/Ne−D_2,[50] and Ar−D_2/F−D_2.[26] The degrees of dissociation obtained with this assumption lie in the range 25−55% and are listed in Table 1.

As mentioned in section II, only fluorine atoms in the $P_{3/2}$ ground state are assumed to take part in the reaction with the ground state D_2 molecules. Under thermal conditions about 77% of the produced atoms are estimated to populate the $^2P_{3/2}$ state at the typical fluorine-source operating temperature of 1150 K. Thus, the density of F atoms in the scattering volume considered in eq 6 has to be multiplied by the factor $\rho_{fs} = 0.77$, in order to account for the actual density of *reactive* F atoms.

On the other hand, the quantum and quasiclassical dynamical calculations with which the experimental results are compared in section IV have been performed for the $\Omega = {}^1/_2$ state PED which adiabatically correlates the ground states of the reactants and the products:

$$F(^2P_{3/2,1/2}) + D_2(^1\Sigma_g^+) \xrightarrow{1^2A'} DF(^1\Sigma) + D(^2S_{1/2})$$

Ω designates here the projection of the $F(^2P_{3/2})$ atom onto the $F-D_2$ axis. Present potential calculations neglect implicitly any contribution to the dynamics of the reaction from the two upper surfaces, $2^2A'$ and $^2A''$, connected asymptotically to the $^2P_{1/2}$ and $^2P_{3/2,3/2}$ states of the separated fluorine/D_2 system, respectively.[18,56,57] Thus, when the result of these calculations is compared with the experimental observations, the calculated cross-sections have been multiplied by a factor of 0.5, equal to the experimental relative population of the $\Omega = {}^1/_2$ fine structure state.

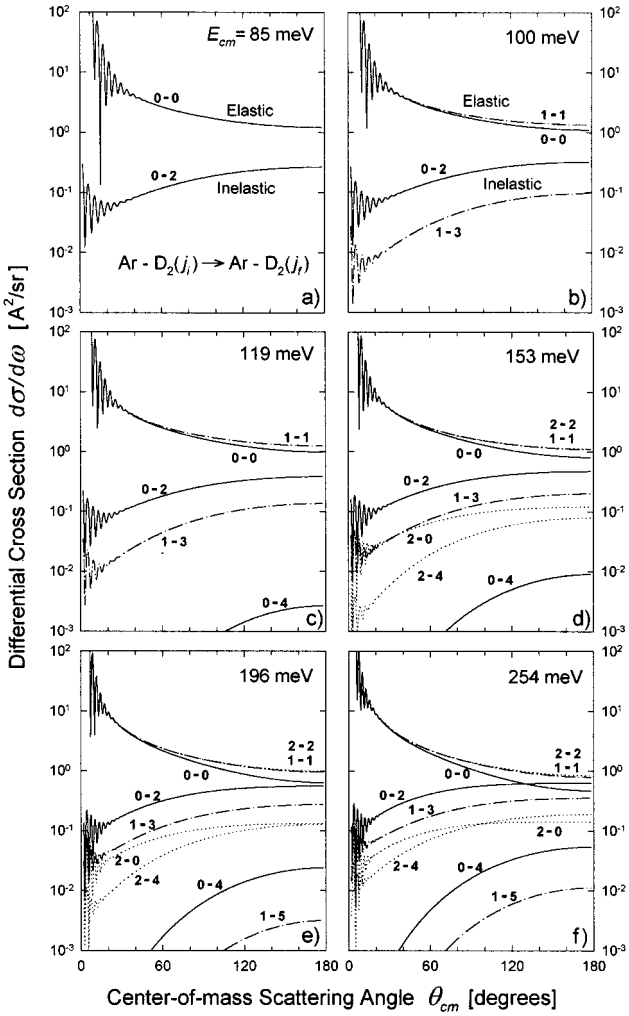

Figure 3. Center-of-mass differential cross-sections for elastic and rotationally inelastic scattering for the system Ar + $D_2(j_i$=0,1,2) → Ar + $D_2(j_f$=0−6) calculated with the coupled-states approximation on the semiempirical potential energy surface of Buck *et al.*[52] at the collision energies of (a) the experiments of Buck *et al*. (85 meV) and (b−f) the present investigation (100−254 meV). The Ar−D_2 cross-sections were used for the absolute calibration of the beam intensities and detection efficiency of the reactive F−D_2 scattering experiments (see text).

The absolute detection efficiency of the mass spectrometer detector is obtained in two steps: (i) The most recent experimental investigations agree on a cross-section for electron impact ionization of the Ar atom, Ar + $e \rightarrow Ar^+ + 2e$, of $\sigma_e(Ar) = (2.6 \pm 0.4) \times 10^{-16}$ cm^2 at the electron energy $E_e = 100$ eV,[58,59] of the present experiments. On the other hand, according to recent calculations of Märk,[60] the cross-section for DF^+ formation is 2.5 times smaller than that for Ar ionization at 100 eV. Although the detection probability of a molecule also depends on the internal rovibrational state, from available experimental ionization data for different vibrational states of HF,[68] these corrections are expected to be smaller than 10−20% for DF vibrational states up to $v_f = 4$ and have been neglected in the analysis. Furthermore, it is assumed that the remaining stages of the detection process, namely, the transmission through the mass spectrometer and the conversion to electrons at the multiplier, are very similar for Ar^+ and DF^+ ions.[61] With these asumptions the relative detection efficiency of (neutral) Ar atoms to DF molecules is estimated to be $\epsilon(Ar)/\epsilon(DF) = 2.5$, with an error of ±25%.

(ii) The calculated absolute differential cross-sections for the elastic and rotationally inelastic scattering of Ar−$D_2(j_i)$ → Ar−

TABLE 3: Experimental Conditions and Characteristic Parameters of the Argon and the Converted Deuterium (90%/10% *ortho*-D_2/*para*-D_2) Supersonic Beams in the Present Investigation of Ar−D_2 Nonreactive Scattering, Which Were Carried Out for the Absolute Calibration of the Apparatus[a]

E_{cm}(Ar−D_2) (meV)	Ar			D_2			$C_{Ar} \equiv I_{Ar}/\hat{I}_{Ar}$ (10^{33} cps·m^{-7}·s)	calibrated F−D_2 expt
	P_0(bar)	T_0(K)	v (m/s)	P_0(bar)	T_0(K)	v (m/s)		
100	2	1145	1125	100	295	2010	4.1	A_2
119	7	1120	1115	220	380	2230	5.4	B_2
153	5	1100	1110	250	500	2600	4.5	C_1
196	5	1120	1105	350	750	3000	5.1	D_1
254	8	1220	1140	350	980	3500	5.1	E_1

[a] The same notation is used as in Table 1. The calibration constants, C_{Ar}, are defined in eq 7.

$D_2(j_f)$ are shown in Figure 3 for the collision energies of the present investigation, E_{cm} = 100−254 meV (because of the greater mass of Ar, E_{cm} is slightly higher than for F−D_2 with the same relative velocity). The cross-sections were calculated employing the coupled-states approximation[62−65] on a potential energy surface constructed empirically by Buck and co-workers from D_2−Ar crossed beam differential scattering experiments.[52] The present calculations were tested by reproducing the calculations and the experimental data of Buck *et al.* at E_{cm} = 85 meV (Figure 3a of the present work and Figure 3 of ref 52).

The differential cross-sections of Figure 3 were then used to simulate the measured time-of-flight spectra by means of eq 5, taking into account the initial rotational populations of the D_2 molecules, as listed in Table 2. The calibration factors $C_{Ar} \equiv I_{Ar}/\hat{I}_{Ar} = n_{Ar}^{\circ} n_{D_2}^{\circ} \epsilon(\mathrm{Ar})$, which scale the simulated to the experimental time-of-flight spectra (eq 7), were determined in each Ar−D_2 scattering experiment and are given in Table 3, where the kinematic conditions and the corresponding F−D_2 experiment are listed.

Figure 4 shows time-of-flight spectra of the scattered Ar atoms measured at several representative scattering angles at E_{cm} = 100 and 196 meV (typically a total of 10 angles were measured at each collision energy), together with the corresponding numerical simulations (solid lines). The good agreement in the location, shape, and relative height of the peaks in the spectra constitutes a consistency test for the calculated differential cross-sections of Figure 3, used for the deconvolution of the detected signal and, consequently, for the determination of the calibration constants, C_{Ar}.

Taking into account the considerations made above, eq 7 takes on the following final form:

$$I_{DF}(\Theta_{lab},\Phi_{lab},t_n) = \frac{n_F^{\circ}}{n_{Ar}^{\circ}} \frac{\epsilon(DF)}{\epsilon(Ar)} \frac{I_{Ar}}{\hat{I}_{Ar}} \hat{I}_{DF}(\Theta_{lab},\Phi_{lab},t_n)$$

$$= \rho_{fs} \frac{0.22\alpha}{1 - 0.11\alpha} \frac{1}{2.5} C_{Ar} \hat{I}_{DF}(\Theta_{lab},\Phi_{lab},t_n) \quad (10)$$

where I_{DF} is the scattering signal detected in the nth time-of-flight channel and $\hat{I}_{DF}$ is the deconvolution integral defined in eq 2. Equation 10 has been used for the evaluation of absolute state-to-state differential cross-sections from the measured time-of-flight spectra.

The erors in absolute cross-sections are then affected mainly by the determination of the *relative* ratio of the densities of F and Ar in the scattering volume, involving the degree of dissociation of fluorine ($\Delta[n_F^{\circ}/n_{Ar}^{\circ}] \sim 15\%$), and by the prediction of the detection efficiency of the DF products *relative* to that of Ar atoms ($\Delta[\epsilon(DF)/\epsilon(Ar)] \sim 25\%$). Thus, the possible experimental error in the *absolute* reactive cross-sections is conservatively estimated to be about 50%. The experimental determination of the *relative* cross-sections at the different collision energies is less demanding and can be done much more accurately. From the uncertainty related to the signal-to-noise ratio in the TOF measurements (typically ∼3−5%), and to possible intensity drifts during the scattering experiments (<10%), the relative error is about 10−15%.

IV. Results and Discussion

IV.A. Absolute Differential Cross-Sections. The best-fit center-of-mass absolute differential cross-sections for individual DF product vibrational states are displayed in Figure 5 for the five collision energies studied, E_{cm} = 90−240 meV. They were obtained by summing eq 4 over all final rotational states:

$$(d\sigma/d\omega)_{v_f}(\theta_{cm}) = \sum_{j_f}\sum_{k} A_k(v_f)\, P(j_f;v_f)\, G_k(\theta_{cm})$$

$$= \sum_{k} A_k(v_f)\, G_k(\theta_{cm}) \quad (11)$$

Also shown are total differential cross-sections which were obtained by summing over all final vibration states. The error bars in Figure 5 are typically about 10% and indicate the estimated uncertainty in the relative ratio between the differential cross-sections for two different vibrational states at an arbitrary scattering angle.[18,23]

The F−D_2 total reactive differential cross-section is greatest, in the order of ≈0.35 Å^2/sr, at the large and intermediate center-of-mass scattering angles (the "backward" and "sideways" scattering, respectively) and are lower but still significant at the small angles ("forward" scattering). Since the present experiment at E_{cm} = 90 meV covered only the backward scattering hemisphere (θ_{cm} > 90°) for all final states of the DF products, the results at this energy were extrapolated to the forward hemisphere using the measurements of Neumark and co-workers at 79 meV,[12] as indicated by the dotted lines in Figure 5a. There it can be seen that the reactive cross-section drops rapidly and vanishes for θ_{cm} < 90°.

With increasing collision energy, the differential cross-section maxima of all product vibrational states shift toward smaller scattering angles. A similar shift of the DCS's toward smaller scattering angles is observed, as well, with increasing product vibrational energy. In fact, the total reactive differential cross-section shows remarkably detailed structures as a function of the CM scattering angle with a series of undulations reflecting the maxima of each of the v_f-resolved DCS's, especially at the higher collision energies studied. At all five collision energies the products in v_f = 0 and 1 are confined to the backward hemisphere (θ_{cm} > 90°), whereas for v_f = 2, 3, and 4 they cover a progressively broader angular region. The excitation of the lower vibrational states v_f = 0−2 becomes more probable as the collision energy increases. The product v_f = 0 could only be detected at $E_{cm} \geq$ 180 meV in the present experiments. Particularly interesting is the observation that the DCS of v_f = 4 is significant at all scattering angles and exhibits a maximum at θ_{cm} = 0° that grows in size with increasing E_{cm}. At collision

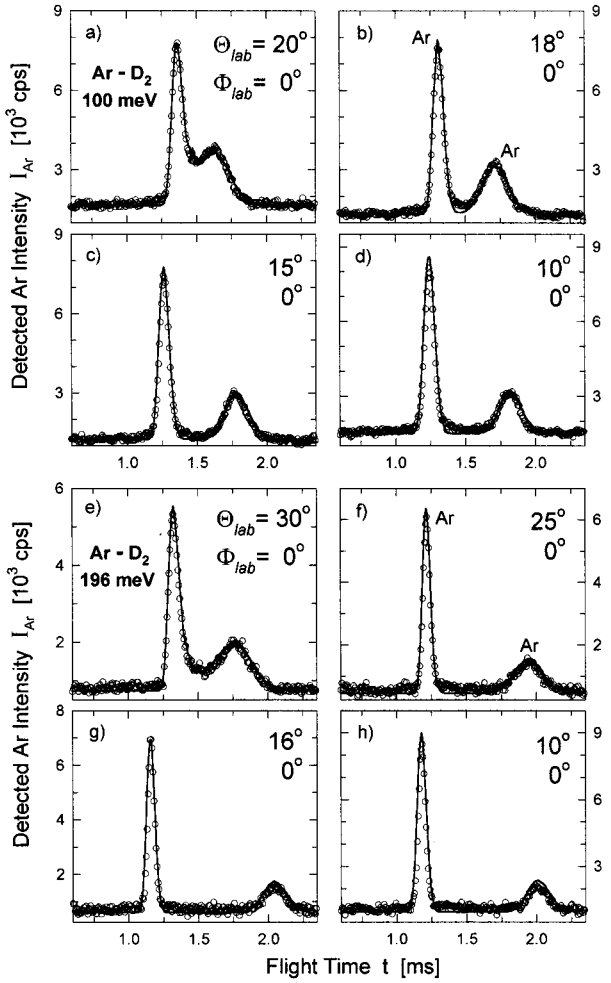

Figure 4. Typical time-of-flight spectra of the Ar atoms scattered by collisions with D_2 molecules at two of the collision energies of the present study: (a−d) E_{cm} = 100 meV; (e−h) E_{cm} = 196 meV. The circles (○) denote the measurements, and the solid curves represent the simulation of each spectrum with the absolute center-of-mass differential cross-sections shown in Figure 3.

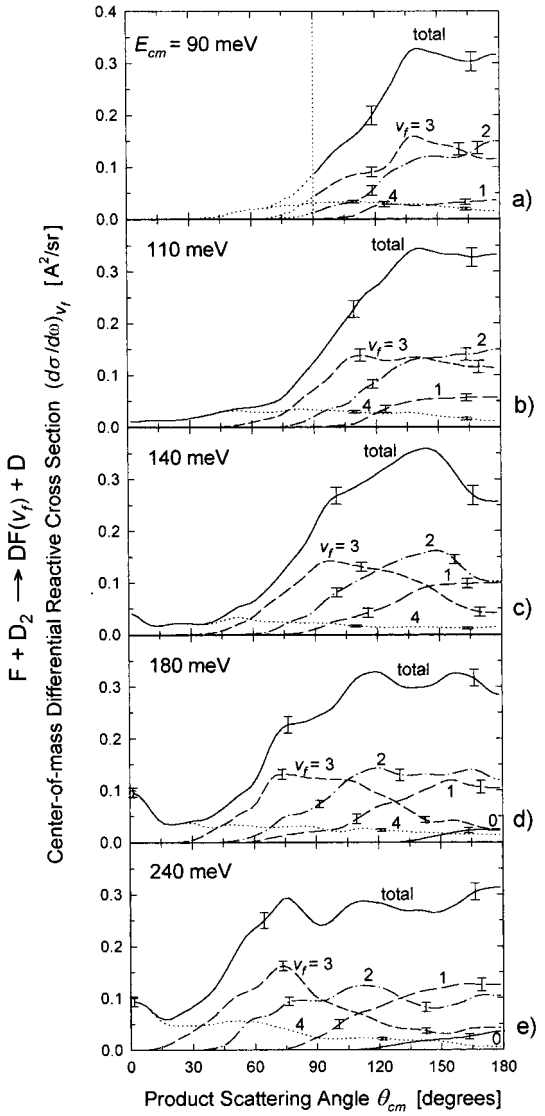

Figure 5. Measured absolute center-of-mass differential cross-sections for the DF product molecules in the vibrational states v_f = 0−4 from F + D_2 reactive scattering at collision energies (a) E_{cm} = 90, (b) 110, (c) 140 meV, (d) 180, and (e) 240 meV. The error bars indicate the estimated experimental uncertainties in the determination of the relative ratio between the differential cross-section of different vibrational states at arbitrary scattering angles, which is typically ~10%. The absolute scale for the experimental data is affected by a possible error as large as 50% (not shown, see text). The present experiment at E_{cm} = 90 meV covers the interval of center-of-mass scattering angles θ_{cm} = 90−180°. The dotted curves for θ_{cm} < 90° in panel a represent the results of ref 12 at 79 meV collision energy.

energies of 140 meV and above, it becomes the global maximum of the DCS for this vibrational product. This forward maximum[12,22] has often been considered as evidence for dynamical resonances.[1,12] In fact, it has been shown in numerous dynamical studies that the magnitude of the reactive DCS at θ_{cm} = 0° is very sensitive to the details of the PES topology.[32,33,36,37,39,41,42,72] The feature explanation in terms of an exclusively quantum type resonance is no longer likely since a a forward peak is also predicted by quasiclassical calculations on the most recent potential energy surfaces for the F−D_2 system.[41,43] Both the quasiclassical and the quantum studies associate the forward scattered products with reactive collisions produced in a narrow interval of large impact parameters.[22,37,43,44] The significant enhancement of the forward scattering in quantum calculation is attributed to tunneling through the centrifugal barrier[44] which accesses larger orbital angular momenta than classically allowed.

IV.B. Total Integral Cross-Sections. The experimental integral, total reactive cross-sections, $\sigma_{tot.}(E_{cm})$, are listed in Table 4 and shown in Figure 6 for all collision energies studied. The results of a previous experiment at E_{cm} = 82.5 meV,[18] which was performed with normal D_2 (a mixture of 66% *ortho*-D_2 and 33% *para*-D_2) at a rotational temperature $T_{rot.}(D_2)$ = 45 K, are also included for comparison. The first value in Table 4 at E_{cm} = 90 meV corresponds to the angular integration of the v_f-resolved DCS's in the restricted CM interval θ_{cm} = 90−180° covered by the present experiment at this particular collision energy. The second entry, given in brackets, corresponds to the integral cross-section estimated for the whole space of scattering angles using the experimental results of Neumark *et al.* at θ_{cm} = 0−90°.[12] The scattering in the forward hemisphere is seen to be only significant for the vibrational states v_f = 3 and v_f = 4, for which it constitutes roughly 10 and 40% of the integral cross-section, respectively. At all higher energies, the present experiments cover the complete range of CM angles and the integral cross-sections are complete. The error bars in Figure 6 correspond to the estimated uncertainty in the determination of the relative cross-section at two different collision energies, i.e., the ratio $\sigma_{tot.}(E_{cm})/\sigma_{tot.}(E'_{cm})$, which, as discussed in section III.B, is about ~10%.

The measured total integral reactive cross-sections increase monotonously in the whole interval of collision energies studied, from 0.80 and 1.5 Å^2 at E_{cm} = 82.5 and 90 meV, respectively,

TABLE 4: Experimental Absolute Total, $\sigma_{tot.}$, and Product Vibrational State Resolved, $\sigma_v(v_f)$, Integral Cross-Sections (Å^2) for the F + D_2 Reaction at the Five Collision Energies of the Present Investigation, E_{cm} = 90−240 meV[a]

	for given E_{cm} (meV)					
	82.5 meV	90 meV	110 meV	140 meV	180 meV	240 meV
$\sigma_v(v_f=0)$					0.02	0.05
$\sigma_v(v_f=1)$	0.01	0.11 [0.11]	0.20	0.35	0.47	0.54
$\sigma_v(v_f=2)$	0.19	0.43 [0.43]	0.63	0.80	0.94	0.98
$\sigma_v(v_f=3)$	0.41	0.61 [0.68]	0.98	1.01	1.04	1.02
$\sigma_v(v_f=4)$	0.19	0.20 [0.28]	0.38	0.26	0.34	0.41
$\sigma_{tot.}$	0.80	1.35 [1.5]	2.2	2.4	2.8	3.0

[a] The results at 82.5 meV are from an earlier experiment.[18] The values listed at 90 meV correspond to the integration of the experimental differential cross-sections in the backward scattering hemisphere, θ_{cm} = 90−180° only. The values in brackets are estimated for all scattering angles (see text). The experimental error in the relative and the absolute integral cross-sections is of 10 and 50%, respectively.

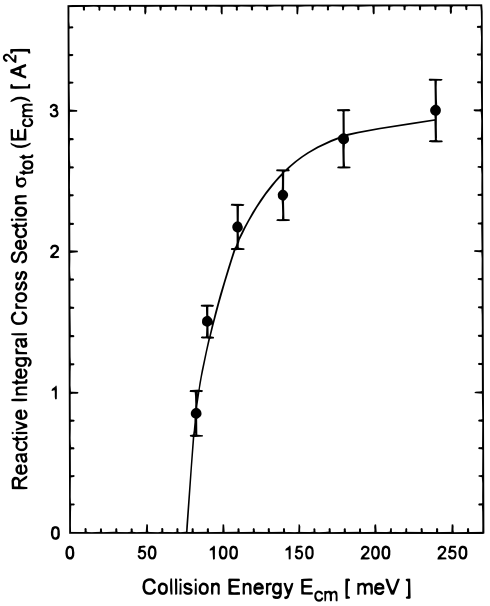

Figure 6. Measured absolute total reactive cross-section for the F + D_2 reaction at the collision energies E_{cm} = 90−240 meV of the present study (●). The cross-section obtained in a previous experiment at 82.5 meV collision energy[18] is also included for comparison. The thicker error bars correspond to the estimated uncertainty in the determination of the relative cross-section at two different collision energies (typically 10%). The systematic calibration uncertainty in the absolute scale of the experimental cross-sections is shown in Figure 7. The solid curve represents the best fit to the measured reactive cross-sections obtained with the modified line-of-centers model given in eq 12.

up to 3.0 Å^2 at E_{cm} = 240 meV (see Figure 6). The increase is especially steep in the low collision energy range, where the ratios $\sigma_{tot.}$(110meV)/$\sigma_{tot.}$(82.5 meV) = 2.75 and $\sigma_{tot.}$(110meV)/$\sigma_{tot.}$(90 meV) = 1.5 are found. At higher energies, the cross-section increases by a factor of only about 1.4 between 110 and 240 meV. The ratio $\sigma_{tot.}$(140meV)/$\sigma_{tot.}$(82.5meV) = 3.0 ± 0.3 obtained in the present study is consistent, within the limits of the estimated experimental uncertainty, with the value of 2.2 ± 0.3 reported by Neumark and co-workers.[12] In making this comparison, however, it must be noted that the D_2 reactants in the latter experiments had different initial rotational distributions than in the present ones.[19]

The data in Figure 6 have been fitted with an expression of the type $\sigma_{tot.}(E_{cm}) = A(E_{cm} - E_0)^n/E_{cm}$ similar to the one predicted by the line-of-centers model (for which n = 1).[1] It has been shown that this function type yields analytically integrable rate constants with standard Arrhenius activation energy E_0.[77] The best fit to the experimental data was obtained with the values E_0 = 0.076 eV and n = 0.72 to give

$$\sigma_{tot.}(E_{cm}) = (18\ \text{Å}^2\cdot\text{meV}^{0.28})(E_{cm} - (76\ \text{meV}))^{0.72}/E_{cm} \quad (12)$$

which provides the best fit (solid-line curve in Figure 6) to the measured values of $\sigma_{tot.}(E_{cm})$. However, the energy threshold obtained from this simple model (~76 meV, or 1.8 kcal·mol^{-1} activation energy) is not satisfactory. According to the low-energy observations of Neumark and co-workers, the threshold for the F + D_2 reaction is expected to be at about 30 meV.[12] In fact, the introduction of steric corrections to the line-of-centers model usually yields a slower concave-upward increase of $\sigma_{tot.}$ with E_{cm} for collision energies near the threshold.[1] It is also conveivable that the threshold is lowered by tunneling effects.

The experimental absolute reactive cross-sections are compared in Table 5 and in Figures 7 and 8 with the results of quantum[21] and quasiclassical[41,43,73] dynamical calculations performed on the two most recent potential energy surfaces, the 6SEC surface[33] and the SW surface by Stark and Werner.[34] The thinner error bars in the figure illustrate the experimental uncertainty in the absolute scale of the cross-sections (50%). The calculated cross-sections have been obtained after averaging the results for the reactions F + D_2(j_i = 0,1,2), from the three lowest rotational states of the D_2 molecule, with the initial populations of the corresponding experiments (Table 2). For energies below 90 meV, the relative populations at 90 meV (90% j_i = 0, 10% j_i = 1) were used to average the calculations. All calculated cross-sections have been additionally multiplied by the factor of 0.5 in order to account for the experimental population of the $P_{3/2,1/2}$ fine-structure state of fluorine which is able to react.

As can be seen in Figure 7, the quantum mechanical predictions for $\sigma_{tot.}$ for both the 6SEC and the SW surfaces lie systematically above the experimental values but are entirely consistent with them within the estimated uncertainty of the absolute cross-sections. This is also true for the quasiclassical cross-sections calculated on the SW PES, which for E_{cm} > 80 meV lie very close to the quantum results on the same PES. In order to compare in more detail the collision energy dependence of the experimental and the QM and QCT calculated cross-sections, the latter ones have been multiplied by a factor of 0.90 in Figure 8a and of 0.82 in Figure 8b to fit the calculated QM curves on the SW and 6SEC surfaces, respectively. The QM and QCT results on both surfaces predict a roughly similar shape and slope for $\sigma_{tot.}(E_{cm})$ over the entire range of collision energies. The dynamical calculations on the SW surface yield cross-sections which are about 10% smaller than the ones on the 6SEC surface. Otherwise, the QM calculations on the two PESs are in excellent agreement with the experimental relative cross-sections in the energy interval presently investigated, E_{cm} = 90−240 meV, as can be seen in Figures 8a,b. The QCT calculations on both surfaces predict only a slightly steeper variation of $\sigma_{tot.}$ with E_{cm} than the respective QM calculations and are also in good agreement with the experiment.

The most significant differences between the different dynamical calculations and between these and the experiment arise in the low collision energy range, E_{cm} < 110 meV. Below 110 meV, the QM and QCT calculations on the SW and 6SEC PES's agree in a much slower decrease toward zero of the reactive cross-section with decreasing collision energy than experimentally observed. In particular, the theoretical values for the ratio $\sigma_{tot.}$(110meV)/$\sigma_{tot.}$(82.5meV) are in all cases about 80% smaller than experimentally observed. Interestingly, the QM calculations on the SW surface even predict the absence of an energy threshold for F−D_2 reaction, in strong contrast

TABLE 5: Integral Cross-Sections (Å²) for the F + D_2 Reaction Resulting from Quantum Mechanical (QM) and Quasiclassical (QCT) Calculations on the Potential Energy Surfaces (PES) SW and 6SEC[a]

	calculation on the SW PES for given E_{cm} (meV)							calculation on the 6SEC PES for given E_{cm} (meV)	
	QCT						QM	QCT	
	83.5 meV[b]	90 meV[c]	110 meV[c]	140 meV[c]	180 meV[d]	240 meV[d]	87 meV[e]	83.5 meV[c]	140 meV[c]
$\sigma_v(v_f=0)$					0.035	0.10			
$\sigma_v(v_f=1)$	0.01	0.02	0.11	0.34	0.54	0.66	0.08	0.003	0.014
$\sigma_v(v_f=2)$	0.33	0.40	0.69	1.00	1.20	1.33	0.63	0.24	0.71
$\sigma_v(v_f=3)$	0.80	0.85	0.95	0.92	0.94	1.03	0.77	0.75	1.39
$\sigma_v(v_f=4)$	0.42	0.42	0.35	0.28	0.27	0.32	0.31	0.63	0.93
$\sigma_{tot.}$	1.56	1.69	2.10	2.54	2.99	3.44	1.79	1.63	3.05

[a] The theoretical cross-sections have been obtained after averaging the results for the reactions F + D_2 (j_i=0,1,2) over the rotational weights of the present experiments (Table 2). All values have been additionally multiplied by the spin−orbit factor of 0.5 corresponding to the experimental population of the fine structure state $^2P_{3/2,1/2}$, not included in any of the calculations (see text). [b] Reference 41. [c] Reference 73. [d] Reference 43. [e] Reference 21.

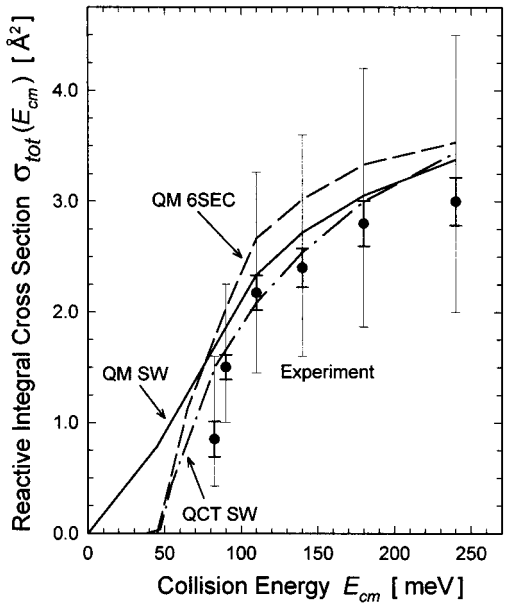

Figure 7. Quantum mechanical (QM) total cross-section for the F + D_2 reaction as a function of collision energy calculated on the SW (solid curve) and 6SEC (dashed curve) potential energy surfaces.[33,35] Also shown is the quasiclassical (QCT) cross-section calculated on the SW PES (dotted−dashed curve). The circles represent the experimental values with the thicker bars showing the relative uncertainty as in Figure 6. The wider, thinner error bars illustrate the systematical absolute calibration error of the experimental cross-sections (50%). All theoretical cross-sections have been obtained after the results for the reactions F + D_2(j_i=0,1,2) have been averaged over the rotational weights of the present experiments (Table 2) and have additionally been multiplied by the spin−orbit factor of 0.5 corresponding to the experimental population of the ground state $^2P_{3/2,1/2}$ of the fluorine atoms (see text).

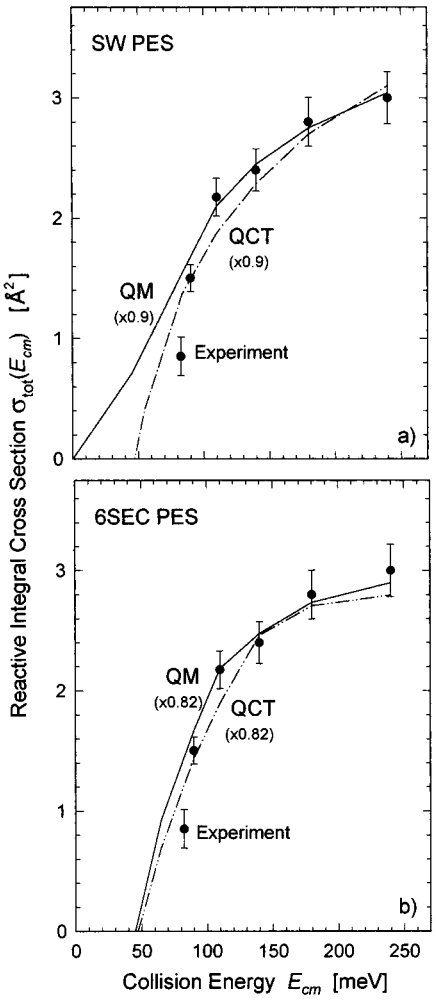

Figure 8. Quantum mechanical (solid curves) and quasiclassical (dotted−dashed curves) total cross-section for the F + D_2 reaction as a function of collision energy calculated on the (a) SW and (b) 6SEC potential energy surfaces. All theoretical values have been globally multiplied by a factor of 0.90 in panel a and of 0.82 in panel b, in order to fit the quantum curves to the experimental data (circles) in each case. The error bars represent the experimental uncertainty in the relative reactive cross-sections.

with all the other theoretical studies including the QCT calculation on the same PES, which agree on a collision energy threshold for reaction at $E_{cm} \approx 40$ meV. Provided that the approximations involved in the quantum treatment[46] work properly at low collision energies, the absence of quantum mechanical reactive threshold on the SW PES is likely to be related to a too low entrance barrier in the F−D−D transition state of this PES. The inclusion of spin−orbit coupling is expected to correct this.[34,44,46]

IV.C. State-Resolved Integral Cross-Sections. The experimental absolute integral cross-sections for the different final vibrational product states, DF(v_f=0−4), are listed in Table 4 and shown in Figure 9. There it can be seen that, whereas the cross-sections for $v_f = 0$, $v_f = 1$, and $v_f = 2$ show a gradual increase with collision energy, for $v_f = 3$, the most probable product state at all energies, the cross-section levels off, remaining approximately constant at ≈1 Å² between 110 and 240 meV. Finally, the integral cross-section for $v_f = 4$ displays the richest structure. At first it grows monotonously, like the rest of vibrational states, until at 110 meV it has a local maximum (0.38 Å²), then decreases sharply, down to about 70% of this value, at 140 meV, and grows slowly again up to a value at 240 meV similar to that at 110 meV (see Table 4).

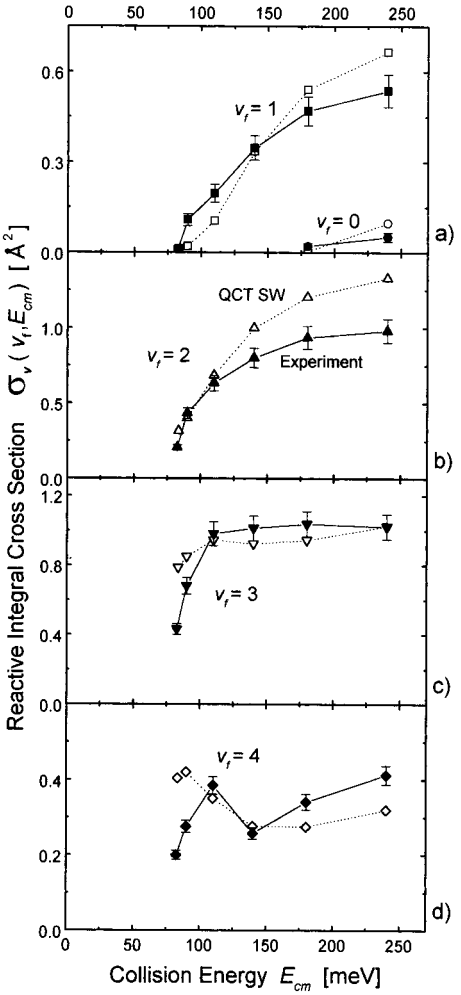

Figure 9. Experimental and QCT calculated integral reactive cross-sections for the DF product molecules in the vibrational states (a) v_f = 0 and v_f = 1, (b) v_f = 2, (c) v_f = 3, and (d) v_f = 4. The present experimental values are shown by solid symbols and solid curves. The quasiclassical calculation on the SW potential energy surface[41,43,73] is shown by unfilled symbols. The experimental data are shown with error bars corresponding to the estimated uncertainty of typically 10% in the determination of the relative cross-section of two different vibrational states at different collision energies.

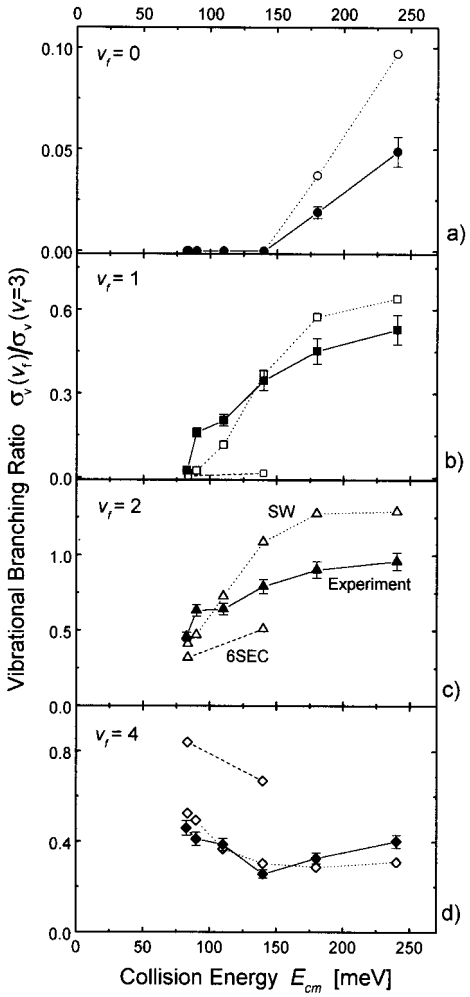

Figure 10. Experimental and QCT calculated vibrational branching ratios, $\sigma_v(v_f)/\sigma_v(v_f=3)$, for the DF product molecules in the vibrational states (a) v_f = 0, (b) v_f = 1, (c) v_f = 2, and (d) v_f = 4. The present experimental values are shown by solid symbols and solid curves. The quasiclassical calculation on the SW potential energy surface[41,43,73] are shown by unfilled symbols and dotted curves. The quasiclassical results on the 6SEC potential energy surface[73] are also shown by unfilled symbols and by dashed curves.

The only available quantum mechanical calculation on the SW PES of v_f-resolved cross-sections has been carried out by Baer and co-workers at E_{cm} = 87 meV (Table 5). The QM cross-sections are in close agreement with the experimental results at 90 meV, the largest discrepancy being for v_f = 2 for which the calculated cross-section is roughly 30% larger than experimentally observed.

In Figure 9 and Table 5 the measured cross-sections are compared with the quasiclassical vibrational cross-sections calculated on the SW PES.[41,43,73] The main trends of the collision energy dependence of the experimental vibrational cross-sections of all final DF(v_f) products are well-reproduced by the QCT calculations. In agreement with the experiment, the quasiclassical study predicts a monotonic growth of the integral cross-section for the lowest vibrational products v_f = 0, 1, and 2 in the entire energy range studied. The calculated curves, however, increase in general more rapidly than the experimental ones, which results in an overestimation of the cross-section of these vibrational states at the highest collision energies (E_{cm} = 140−240 meV). In particular, v_f = 2 is the most probable product state in the QCT calculation for energies above 140 meV, in contrast to the experiment in which v_f = 3 represents the largest cross-section for all the collision energies studied. The QM results for $\sigma_v(v_f)$ on the SW PES reported by Baer *et al.*[21] do not seem to correct for this deficiency but yield even larger relative cross-sections for v_f = 1 and v_f = 2. For instance, the branching ratio $\sigma_v(v_f=2)/\sigma_v(v_f=3)$ is roughly a factor of 1.7 larger in the QM calculation at 87 meV than in the QCT one at 90 meV (Table 5). On the other hand, the QCT calculations on the SW PES give the best agreement with the cross-section for v_f = 3, which levels off at about 1.0 Å^2 for $E_{cm} \geq$ 110 meV. As for the highest vibrational product accesible, v_f = 4, the QCT integral cross-section decreases smoothly with increasing E_{cm} and falls slowly down to a roughly constant value of about 0.3 Å^2 for $E_{cm} \geq$ 140 meV. A qualitative discrepancy between the theoretical curve and the experimental data for v_f = 4 arises in the low collision energy range, E_{cm} = 82.5−110 meV, where the measured cross-section increases by a factor of about 2, in contrast to the decreasing trend predicted by the QCT calculation.

As can be seen in Figure 10, the measured vibrational branching ratios, $\rho_v(v_f) \equiv \sigma_v(v_f)/\sigma_v(v_f=3)$, vary considerably with collision energy. At E_{cm} = 110 meV, for example, $\rho_v(v_f=1)$ = 0.20 (0.12) and $\rho_v(v_f=2)$ = 0.64 (0.73), whereas these same ratios at 240 meV are $\rho_v(v_f=1)$ = 0.53 (0.64) and $\rho_v(v_f=2)$ = 0.96 (1.29), where the values in brackets are the quasiclassical branching ratios obtained on the SW PES. The QCT vibrational

TABLE 6: Effective Rate Constant, $k_{eff}(T)$, Evaluated with the Modified Line-of-Centers Model of Equation 12 to Fit the F−D_2 Reactive Cross-Sections Measured in the Present Work[a]

	this work	bulk expts		theory	
T (K)	k_{eff} (T)	HBGM[b]	WH[c]	QM SW PES[d]	QCT SW PES[e]
300	0.5	1.4	1.4	1.5	1.1
500	1.8	3.2	(3.0)	3.0	2.7
700	3.13	4.5	(4.1)		
1000	4.9	(5.8)	(5.2)		
1500	7.2	(7.1)	(6.3)		

[a] The results for thermal rate constans obtained in previous experiments and dynamical calculations are included for comparison. The values in brackets are the result of a high-temperature extrapolation of the measured data. All rate constant are in units of 10^{-11} cm^3/s. [b] Reference 4. [c] Reference 3. [d] Reference 46. [e] Reference 47.

branching ratios on the SW PES are in general in good agreement with the experiment, especially for $v_f = 4$ (see Figure 10). However, significant differences between the QCT results and the experiment are also found. For instance, the QCT calculation on the SW surface overestimates $\rho(v_f=2)$ by as much as ∼30% at collision enegies above 140 meV. On the other hand, the calculation on the 6SEC surface predicts correctly $v_f = 3$ as the most probable vibrational product at the two collision energies where theoretical data are available (83.5 and 140 meV). However, it largely overestimates the cross-section for $v_f = 4$ and, underestimates it for $v_f = 1$. At 140 meV, for instance, the QCT branching ratios $\rho(v_f=4) = 0.67$ and $\rho(v_f=1) = 0.01$, calculated on the 6SEC PES, differ significantly from the experimental values of 0.26 and 0.35, respectively.

IV.D. Reaction Rate Constants. The availability of absolute reactive cross-sections makes it possible also to calculate rate constants, thus providing a direct link between the dynamical (single collision) and the kinetical (bulk) studies on this reaction. An effective specific rate constant, $k_{eff}(T,\{j_i\})$, can be obtained by means of the following well known expression:[1,74−76]

$$k_{eff}(T,\{j_i\}) \approx \left(\frac{8k_BT}{\pi\mu}\right)^{1/2} \frac{1}{(k_BT)^2}\int_0^\infty dE_{cm}\, E_{cm} e^{-E_{cm}/(k_BT)}\sigma_{tot.}(E_{cm}) \quad (13)$$

In eq 13 k_B is the Boltzmann constant and μ is the reduced mass of the reactants F−D_2. $\{j_i\}$ denotes the initial rotational populations of the D_2 reactants in the present experiments. k_{eff} can be calculated with the analytic fit of the measured values of $\sigma_{tot.}(E_{cm})$ given in eq 12. For $T = 700$, 1000, and 1500 K, eq 13 yields the effective rate constants: k_{eff} (700,1000,1500K) = 3.13, 4.9, and 7.2 × 10^{-11} cm^3/s, respectively, as listed in Table 6.

Since $j_i = 0$ is the most populated rotational state of the D_2 reactants in the present experiments (see Table 2), $k_{eff}(T,\{j_i\})$ is expected to resemble the rate constant of the reaction F + $D_2(v_i=0,j_i=0)$, but not the thermal rate constant, $k(T)$. Rather, the value of k_{eff} is expected to be systematically lower than the thermal rate constant at the same temperature, since previous experimental studies at collision energies 140−240 meV [20,22,23,41] have shown that the reactivity of the F + $D_2(j_i)$ system is markedly enhanced by D_2 reactants in the rotational excitation. This can be seen in Table 6, where at $T = 300$ K the thermal rate constants obtained in previous experiments,[3,4] as well as those predicted in QM and QCT calculations on the SW PES[46,47] are typically about 2 to 3 times larger than those evaluated in the present work. As mentioned above, it is actually not so surprising to find such a large discrepancy at low temperatures. First, since collision energies below 80 meV, i.e., outside the range included in the present work, contribute roughly 85% to the thermal energy distribution at 300 K; the rate constant estimated at this temperature is very sensitive to the assumed excitation function near the reaction threshold (E_{cm} < 80 meV). Second, it is in the vicinity of the threshold where the largest differences in cross-section arise between the reaction from the excited rotational states of D_2 in comparison with the reaction F + $D_2(j_i=0)$ from the ground state.[46,47]

The effect of the enhancement of the F + D_2 reactivity on the calculated rate constant at low temperature can be illustrated by computing the specific rate constant, $k_{eff}(T,\{j_i\}$, with the QCT cross-sections calculated on the SW PES (see Figure 7) which are weighted over the experimental initial rotational populations of the D_2 reactants ($\rho(j_i=0) = 90\%$ at $E_{cm} \le 110$ meV). The use of the quassiclassical reactive cross-sections for $\sigma_{tot.}(E_{cm})$ in eq 13 leads to $k_{eff}^{QCT}(T) = 0.6 \times 10^{-11}$ and 1.7×10^{-11} cm^3/s at $T = 300$ and 500 K, respectively. These values are almost a factor of two smaller than the thermal rate constants obtained in the same calculation including all initial j_i states of D_2 with significant thermal populations (Table 6), and are in excellent agreement with the values evaluated in the present work (0.6 × 10^{-11} and 1.8 × 10^{-11} cm^3/s, respectively).

Notably, a much better concordance between the present k_{eff} and the previously reported rate constants is found at higher temperatures. At $T = 700$ K, $k_{eff}(T)$ is typically 30% smaller than the measured thermal rate constants (see Table 6). At $T = 1000$ K this difference reduces to 15%, which roughly coincides with the relative size of the cross-sections for the reactions F + $D_2(j_i=2)$ and F + $D_2(j_i=0)$ predicted by the dynamical calculations on the SW surface[46,47] at collision energies far above the threshold.

V. Summary and Conclusions

Absolute differential and integral cross-sections have been evaluated for the DF(v_f=0−4) vibrational products from the reaction F + $D_2(v_i=0,j_i=0-2)$ → DF(v_f) + F at five collision energies in the range 90−240 meV. The beam intensities and detection efficiency were calibrated with the aid of an additional Ar−D_2 scattering experiment for which an accurate Ar−D_2 potential energy surface is available. In addition only the *relative* atom density in the F_2 beam, $n_F°/n_{Ar}°$, and the *relative* detection efficiency, $\epsilon(DF)/\epsilon(Ar)$, have to be determined. The systematic experimental overall error in the absolute value of the F−D_2 cross-sections is estimated to be less than 50%. On the other hand, the relative cross-sections are affected by much smaller errors, of typically 10%.

At all collision energies investigated, the largest values of the center-of-mass differential cross-section for F−D_2 reactions are observed in the backward scattering hemisphere in which the DF products are scattered in a direction opposite to that of the incoming F atom. Such behavior is characteristic of a direct reaction with a narrow opacity function (maximum inpact parameter ∼ 1.5 Å^2).[43] However, as the collision energy of the reactants increases between 90 and 240 meV and progressively larger impact parameters become accessible, the DF products in all final rovibrational states tend to cover a broader range of scattering angles, including the forward direction. In particular, the cross-section for the highest excited vibrational product state, $v_f = 4$, shows a distinct maximum for forward scattering ($\theta_{cm} = 0°$) at collision energies above 110 meV (see Figure 5). This behavior, which is observed experimentally only for $v_f = 4$,[12,22] has often been considered as evidence for quantum resonances.[1,12] This explanation is now no longer considered to be correct since it is also predicted by quasiclassical calculations on the most recent potential energy

surfaces.[41,43] Dynamical, essentially classical resonances in product vibration states are still an open option for the observed features. Both the quantum and the quasiclassical studies associate the forward scattered products with reactive collisions in a narrow interval of large impact parameters.[22,37,43,44]

The total reactive cross-section undergoes a sharp increase with the collision energy, from 0.80 Å^2 at 82.5 meV[18] and 1.5 Å^2 at 90 meV up to 3.0 Å^2 at 240 meV, which can be empirically described with a modified line-of-centers model (see Figure 6). The behavior of the reactive cross-section in the interval of collision energies of 90−240 meV is in excellent agreement with the prediction of quantum mechanical and quasiclassical calculations on the 6SEC and SW potential energy surfaces. The calculated absolute cross-sections are typically 10% larger on the SW PES and 20% larger on the 6SEC PES than the experimental values but are always within the experimental uncertainty of the absolute calibration of the apparatus (50%).

The increase of the experimental cross-section is particularly steep at low collision energies ($E_{cm} \leq 110$ meV). Compared to the experiment, the quantum cross-sections on the SW PES display an unrealistically slow variation and yield significant reaction cross-section values for all collision energies $E_{cm} > 0$ meV (Figures 8 and 9). This absence of a collision energy threshold for reaction is apparently related to a too low entrance barrier in the SW surface, which is partially expected because of the neglected spin−orbit coupling.[34,44,46]

The measured absolute reactive cross-sections yield effective rate constants ranging at $k_{eff}(300-1500\ K) = (0.5-7.2) \times 10^{-11}$ cm^3/s (Table 6), which are smaller than the thermal rate constants. It is shown that the difference is compatible with the much lower population of rotationally excited states in the scattering experiments.

Except for these deficiencies at low collision energy, overall, the SW potential energy surface is found to perform well at collision energies above 90 meV. In particular, QCT dynamics describes with reasonable accuracy the magnitude as well as the collision energy and the final vibrational state dependence of the F + D_2 reactive cross-section, at least up to $E_{cm} = 240$ meV.

Acknowledgment. We are grateful to F. J. Aoiz, V. J. Herrero, and L. Bañares (Madrid, Spain) for giving us their QCT results prior to publication. We thank the Madrid group as well as M. Baer (Yavne, Israel) for many fruitful discussions on the significance of the results presented in this paper and J. Pick for technical assistance throughout the experiments. The work of L.Y.R. in Göttingen was financed by a grant of the Deutsche Forschungsgemeinschaft. B.M.-H. acknowledges support from the Human Capital and Mobility Programme of the EU.

References and Notes

(1) Levine, R. D.; Bernstein, R. B. *Molecular Reaction Dynamics and Chemical Reactivity*; Oxford University: New York, 1987. See also references cited therein.
(2) Anderson, J. B. *J. Chem. Phys*. 1970, *52*, 3849.
(3) Wurzberg, E.; Houston, P. L. *J. Chem. Phys*. 1980, *72*, 4811.
(4) Heidner, R. F.; Bott, J. F.; Gardner, C. E.; Meizer, J. E. *J. Chem. Phys*. 1980, *72*, 4815.
(5) Cohen, N.; Westberg, K. R. *J. Phys. Chem. Ref. Data* 1983, *12*, 531.
(6) Stevens, P. S.; Brunes, W. H.; Anderson, J. G. *J. Phys. Chem.* 1989, *93*, 4068.
(7) Polanyi, J. C.; Wooddall, K. B. *J. Chem. Phys.* 1972, *57*, 1575.
(8) Jonathan, N.; Melliar-Smith, C. M.; Slater, D. H. *Mol. Phys*. 1971, *20*, 93.
(9) Kompa, K. L.; Parker, J. H.; Pimentel, G. C. *J. Chem. Phys.* 1968, *49*, 4257.
(10) Parker, J. H.; Pimentel, G. C. *J. Chem. Phys*. 1969, *51*, 91.
(11) Berry, M. J. *J. Chem. Phys.* 1973, *59*, 6229.
(12) Neumark, D. M.; Wodtke, A. M.; Robinson, G. N.; Hayden, C. C.; Lee, Y. T. *J. Chem. Phys.* 1985, *82*, 3045. Neumark, D. M.; Wodtke, A. M.; Robinson, G. N.; Hayden, C. C.; Shobatake, K.; Sparks, R. K.; Schafer, T. P.; Lee, Y. T. *J. Chem. Phys.* 1985, *82*, 3067.
(13) Faubel, M.; Schlemmer, S.; Sondermann, F.; Toennies, J. P. *J. Chem. Phys*. 1991, *94*, 4676.
(14) Schlemmer, S. Ph.D. Thesis, University of Göttingen, 1991; Max-Planck-Institut für Strömungsforschung, Bericht 3, 1992.
(15) Sondermann, F. Ph.D. Thesis, University of Göttingen, 1992; Max-Planck-Institut für Strömungsforschung, Bericht 5, 1993.
(16) Tappe, U. Diplom Thesis, University of Göttingen, 1992.
(17) Faubel, M.; Rusin, L. Y.; Schlemmer, S.; Sondermann, F.; Tappe, U.; Toennies, J. P. *J. Chem. Soc., Faraday Trans*. 1993, *89*, 1475.
(18) Faubel, M.; Rusin, L.; Schlemmer, S.; Sondermann, F.; Tappe, U.; Toennies, J. P. *J. Chem. Phys*. 1994, *101*, 2106.
(19) Faubel, M.; Martínez-Haya, B.; Rusin, L. Y.; Tappe, U.; Toennies, J. P. *Z. Phys. Chem.* 1995, *188*, 197.
(20) Faubel, M.; Martínez-Haya, B.; Rusin, L. Y.; Tappe, U.; Toennies, J. P. *Chem. Phys. Lett.* 1995, *232*, 197.
(21) Baer, M.; Faubel, M.; Martínez-Haya, B.; Rusin, L. Y.; Tappe, U.; Toennies, J. P.; Stark, K.; Werner, H.-J. *J. Chem. Phys.* 1996, *104*, 2743.
(22) Faubel, M.; Martínez-Haya, B.; Rusin, L. Y.; Tappe, U.; Toennies, J. P.; Aoiz, F. J.; Bañares, L. *Chem. Phys.* 1996, *207*, 227.
(23) Martínez-Haya, B. Ph.D. Thesis, Universidad Complutense Madrid, June 1996. Published by the Max-Planck-Institut für Strömungsforschung, Göttingen, 1996, Bericht 101, 1996. ISSN-0436-1199.
(24) Baer, M.; Faubel, M.; Martínez-Haya, B.; Rusin, L. Y.; Tappe, U.; Toennies, J. P. Manuscript submitted to *J. Chem. Phys.*
(25) Faubel, M.; Rusin, L. Y.; Schlemmer, S.; Sondermann, F.; Tappe, U.; Toennies, J. P. *J. Chem. Soc., Faraday Trans*. 1993, *89*, 1475, and references cited therein.
(26) Gianturco, F. A.; Ragnetti, F.; Faubel, M.; Martínez-Haya, B.; Rusin, L. Y.; Sondermann, F.; Tappe, U. *Chem. Phys*. 1995, *200*, 405.
(27) Weaver, A.; Neumark, D. M. *Faraday Discuss. Chem. Soc*. 1991, *91*, 5.
(28) Bradforth, S. E.; Arnold, D. W.; Neumark, D. M.; Manolopoulos, D. E. *J. Chem. Phys*. 1993, *99*, 6345.
(29) Manolopoulos, D. E.; Stark, K.; Werner, H.-J.; Arnold, D. W.; Bradforth, S. E.; Neumark, D. M. *Science* 1993, *262*, 1852.
(30) Polanyi, J. C.; Schreiber, J. L. *Faraday Discuss. Chem. Soc*. 1977, *62*, 267.
(31) Schaefer, H. F., III. *J. Phys. Chem.* 1985, *89*, 5336.
(32) Muckerman, J. T. In *Theoretical Chemistry: Advances and Perspectives*; Eyring, H., Henderson, D., Eds.; Academic: New York, 1981; Vol. 6A, pp 1−77, and references cited therein.
(33) Mielke, S. L.; Lynch, G. C.; Truhlar, D. G.; Schwenke, D. W. *Chem. Phys. Lett.* 1993, *213*, 10. Erratum. *Chem. Phys. Lett*, 1994, *217*, 173.
(34) Stark, K.; Werner, H.-J. *J. Chem. Phys.* 1996, *104*, 6515.
(35) Aoiz, F. J.; Bañares, L.; Herrero, V. J.; Sáez Rábanos, V.; Stark, K.; Werner, H.-J. *Chem. Phys. Lett*. 1994, *223*, 215.
(36) Aoiz, F. J.; Bañares, L.; Herrero, V. J.; Sáez Rábanos, V. *Chem. Phys.* 1994, *187*, 227.
(37) Aoiz, F. J.; Bañares, L.; Herrero, V. J.; Sáez Rábanos, V. *Chem. Phys. Lett*. 1994, *218*, 422.
(38) Aoiz, F. J.; Bañares, L.; Herrero, V. J.; Sáez Rábanos, V. *Chem. Phys.* 1994, *187*, 227.
(39) Azriel, V. M.; Billing, G. D.; Rusin, L. Y.; Sevryuk, M. B. *Chem. Phys*. 1995, *195*, 243.
(40) Rosenman, E.; Persky, A. *Chem. Phys.* 1995, *195*, 291.
(41) Aoiz, F. J.; Bañares, L.; Herrero, V. J.; Sáez Rábanos, V.; Stark, K.; Werner, H.-J. *J. Phys. Chem.* 1994, *98*, 10665.
(42) Aoiz, F. J.; Bañares, L.; Herrero, V. J.; Sáez Rábanos, V.; Stark, K.; Werner, H.-J. *J. Phys. Chem.* 1995, *102*, 9248.
(43) Aoiz, F. J.; Bañares, L.; Faubel, M.; Martínez-Haya, B.; Rusin, L. Y.; Tappe, U.; Toennies, J. P. *Chem. Phys*. 1996, *207*, 245.
(44) Castillo, J. F.; Manolopoulos, D. E.; Stark, K.; Werner, H. J. *J. Chem. Phys.* 1996, *104*, 6531.
(45) Rosenman, E.; Hochman-Kowal, S.; Persky, A.; Baer, M. *Chem. Phys. Lett*. 1995, *239*, 141.
(46) Rosenman, E.; Hochman-Kowal, S.; Persky, A.; Baer, M.; Szichman, H. *Chem. Phys. Lett.* 1996, *257*, 421.
(47) Aoiz, F. J.; Bañares, L.; Herrero, V. J.; Stark, K.; Werner, H.-J. *Chem. Phys. Lett*. 1996, *254*, 341.
(48) Faubel, M.; Martínez-Haya, B.; Rusin, L. Y.; Tappe, U.; Toennies, J. P. *J. Phys. D: Appl. Phys.* 1996, *29*, 1885.
(49) Pollard, J. E.; Trevor, D. J.; Lee, Y. T.; Shirley, D. A. *J. Chem. Phys*. 1982, *77*, 4818.
(50) Faubel, M.; Gianturco, F. A.; Ragnetti, F.; Rusin, L. Y.; Sondermann, F.; Tappe, U.; Toennies, J. P. *J. Chem. Phys.* 1994, *101*, 8800.
(51) See, for example, the Newton diagram in Figure 1 of ref 20, describing the kinematics for F−D_2 reactive scattering.
(52) Buck, U.; Meyer, H.; LeRoy, R. J. *J. Chem. Phys.* 1984, *80*, 5589.
(53) Kaye, G. W. C.; Laby, T. H. *Tables of Physical and Chemical Constants*; Longman: London, 1973.

(54) Bird, G. A. *Phys. Fluids* 1976, *19*, 1486.
(55) Beam Dynamics Inc., Type 2 skimmers (Nickel), Minneapolis, MN.
(56) Truhlar, D. G. *J. Chem. Phys.* 1972, *56*, 3189.
(57) Muckerman, J. T.; Newton, M. D. *J. Chem. Phys.* 1972, *56*, 3191.
(58) Stephan, K.; Helm, H.; Märk, T. D. *J. Chem. Phys.* 1980, *73*, 3763.
(59) Wetzel, R. C.; Baiocchi, F. A.; Hayes, T. R.; Freund, R. S. *Phys. Rev. A* 1987, *35*, 559.
(60) Märk, T. D. Private communication (nonpublished calculations of absolute cross-sections for DF ionization by electron impact).
(61) Smith, A. B. *Electron Tube and Microelectronics Division*; EMI Electronics Ltd.: Middlesex, England, ref R. PO34Y72.
(62) Pack, R. T. *J. Chem. Phys.* 1974, *60*, 633.
(63) McGuire, P.; Kouri, D. J. *J. Chem. Phys.* 1974, *60*, 2488.
(64) Kouri, D. J.; Mc,Guire, P. *Chem. Phys. Lett.* 1974, *9*, 414.
(65) Gianturco, F. A. *The Transfer of Molecular Energies by Collisions*; Springer: Berlin, 1979.
(66) Faubel, M.; Schlemmer, S.; Sondermann. F.; Wick, O. In *Proceedings of the 17th International Symposium on Rarified Gas Dynamics*; Beyligh, A. E., Ed.; VCH Verlag: Weinheim, Germany, 1991; p 1490.
(67) Scoles, G. *Atomic and Molecular Beam Methods*; Oxford University Press: New York, 1988; Vol. 1.
(68) Rubahn, H. G.; Toennies, J. P.; Wilde, M.; Wanner, J. *Chem. Phys. Lett.* 1985, *120*, 11.
(69) Aquilanti, V.; Candori, R.; Cappelletti, D.; Luzzatti, E.; Pirani, F. *Chem. Phys.* 1990, *145*, 293.
(70) Fitch, W. L.; Sauter, A. D. *Anal. Chem.* 1983, *55*, 832.
(71) Robinson, G. N.; Continetti, R. E.; Lee, Y. T. *J. Chem. Phys.* 1990, *92*, 275.
(72) Launay, J. M.; Le Dourneuf, M. *ICPEAC XVII* Brisbane; McGillivray, W. R., McCarthy, I. E., Standage, M. C., Eds.; Adam Hilger: England, 1992; p 549. Launay, J. M. *Theor. Chim. Acta* 1991, *79*, 183.
(73) Aoiz, F. J.; Bañares, L.; Martínez-Haya, B.; Stark, K.; Werner, H.-J. Manuscript in preparation.
(74) Eliason, M.; Hirschfelder, J. O. *J. Chem. Phys*. 1959, *30*, 1426.
(75) Karplus, M.; Porter, R. N.; Sharma, R. D. *J. Chem. Phys*. 1965, *43*, 3259.
(76) Laidler, K. J. *Chemical Kinetics*, 3rd ed.; Harper & Row: New York, 1987.
(77) LeRoy, R. L. *J. Phys. Chem.* 1969, *73*, 4338.